JOURNAL OF CATALYSIS **178,** 668–678 (1998)
ARTICLE NO. CA982186

Catalytic Combustion of Ethane over Palladium Foil in the 300–450°C Range: Kinetics and Surface Composition Studies

Claude Descorme,[1] Peter W. Jacobs, and Gabor A. Somorjai

Department of Chemistry and Materials Science Division, E.O. Lawrence Berkeley National Laboratory, University of California Berkeley, Berkeley, California 94720-1460

Received December 2, 1997; revised June 8, 1998; accepted June 22, 1998

Catalytic oxidation of ethane over palladium foils was studied and the kinetic parameters were determined for the reaction. The studies were carried out at 800 Torr total pressure over a wide range of reaction conditions in the temperature range of 300–425°C. The catalyst surface composition was characterized before and after reaction by Auger electron spectroscopy (AES). While we detected only metallic palladium before reaction, the postreaction analysis showed significant formation of PdO_x, a surface oxide, at all temperatures and under all ethane/oxygen ratios. The catalyst that exhibits optimum combustion activity is the one covered with 0.3 to 0.5 monolayer of oxygen. Carbon monoxide temperature-programmed desorption (CO-TPD) was used to evaluate the surface area of the metallic and oxidized palladium in order to normalize the measured catalytic reaction rates. The turnover rate for ethane combustion is in the range of 1–260 s^{-1} (molecule(s) of CO_2 produced per surface palladium atom per second) in the studied temperature range. Under stoichiometric reaction conditions at 325°C the rate for ethylene combustion is 100 times faster than that of ethane and the turnover rate for ethylene formation is calculated to be 0.6 s^{-1} (molecule(s) of C_2H_4 produced per surface palladium atom per second). At 325°C the kinetic orders are 1, 0, and −1 for ethane, carbon dioxide, and water, respectively. The order in oxygen is −1/2 under stoichiometric and fuel-rich conditions and 0 under oxidizing conditions. Apparent activation energies of 104, 116, and 189 kJ/mol under fuel lean, stoichiometric, and fuel-rich conditions, respectively, were observed. While CO_2 is the main carbonaceous product, unoxidized and partially oxidized species, methane and ethylene, are produced in small amounts. The product distribution is typically 98.6 mol% CO_2, 0.9 mol% C_2H_4, and 0.5 mol% CH_4 at 10% conversion during a reaction at 350°C under stoichiometric conditions.

1. INTRODUCTION

Total oxidation of hydrocarbons is carried out primarily for chemical energy conversion to heat or other forms of energy. Catalytic combustion was first introduced by Davy in 1817 (1, 2) and research in this field has expanded greatly since the 1970s (3, 4) during the energy crisis and with growing concerns with NO_x emissions that are the by-products of combustion and whose formation are exponentially dependent on the combustion temperature. Presently catalytic combustion is utilized for both energy generation (5, 6) and for the removal of pollutants (7, 8). Furthermore, it may be used to produce valuable chemicals such as synthesis gas and ethylene. Of the latter there are only two processes for the oxidation of alkanes currently utilized on the scale of commodity chemicals: (1) the production of synthesis gas (CO and H2) from the direct oxidation of methane or some other hydrocarbon source; (2) the oxidation of butane to form maleic anhydride (9, 10).

We undertook a surface science and model catalyst study of ethane combustion and our findings are described in this paper. Palladium polycrystalline foils of about 0.5 cm^2 area were used as catalysts in the temperature range of 300–450°C using total pressure of 1 atm. The ethane to oxygen reactant ratio was adjusted so we could explore the reaction kinetics under (a) stoichiometric ($C_2H_6 : O_2 = 1 : 3.5$), (b) fuel-lean ($C_2H_6 : O_2 < 1 : 3.5$), and (c) fuel-rich ($C_2H_6 : O_2 > 1 : 3.5$) conditions. The catalyst was cleaned in ultra high vacuum (UHV) and its surface composition was monitored in UHV by Auger electron spectroscopy (AES) before and after reaction.

Heterogeneous catalysts for the combustion of alkanes usually consist of either noble metals (for complete oxidation) or metal oxides (for partial oxidation.) Among hydrocarbons, the oxidation of methane has been the most studies because of its great abundance. It is also an undesirable emission in the incomplete combustion in automobile engines and power plants. Although it is generally accepted that rhodium and platinum are more efficient combustion catalysts in the case of high hydrocarbons (C_{2+}), palladium, or rather palladium oxide, is considered to be the best catalyst for the combustion of methane (2–4, 11).

The rate-determining step for the catalytic oxidation of methane and other alkanes is generally considered to be the initial cleavage of the C-H bond, which occurs during or directly after adsorption (5, 11–16). This conclusion is

[1] Corresponding author. E-mail: descorme@leedto.lbl.gov.

0021-9517/98 $25.00

reached because the rate of oxidation is almost always first order in fuel and the fact that light alkenes and oxygenates almost always burn faster than the corresponding alkanes. The rate of combustion correlates with C-H bond strength (2, 4, 12, 17, 18). Under most conditions, the rate of combustion is inhibited by the water and sometimes carbon dioxide (11, 12, 19). In the combustion of methane over supported noble metal catalysts the rate was seen to be independent of oxygen at high oxygen partial pressure, but of negative order under low oxygen partial pressures (2, 17, 20).

2. EXPERIMENTAL

Experiments were performed in an UHV surface analysis chamber equipped with a high pressure cell so as to be able to perform reactions at atmospheric pressure. The chamber is pumped with a liquid nitrogen trapped Varian diffusion pump. The pressure inside the chamber is measured with a Varian hot filament ion gauge. The ultimate base pressure after bake out is 5×10^{-10}Torr (1Torr $= 133.3\ \mathrm{N \cdot m^{-2}}$) and the working base pressure is about 2×10^{-9}Torr.

The chamber is equipped with a Varian 4 grid Retarding Field Analyzer (RFA) and a Varian glancing angle electron gun for AES. Spectra were recorded as [d(number of electrons)/d(voltage)] vs voltage. Net crystal currents were 2 to 10 μA and the electron beam voltage was 2 kV. The peak-to-peak oscillation on the retarding grid voltage was generally kept at $\sim$4 V.

A Balzers QMA 400 quadrupole mass spectrometer was used for residual gas analysis and thermal desorption experiments. The mass spectrometer was equipped with a shroud and a nozzle in order to minimize the gas signal from other parts of the manipulator that heat and desorb gasses during temperature-programmed desorption (TPD). The end of the nozzle is 1/4 in. in diameter and sat 3.5 cm from the sample. Mass spectral data were acquired with a Balzers QMG 421 C controller and Quadstar software was used to analyze the data. Low pressures of gas (10^{-9} to 10^{-4} Torr) could be introduced into the chamber via a Varian leak valve with 1/4 in. stainless steel tubing doser.

Generally Auger spectra were taken on the "front" side of the sample while TPD experiments were performed on the "back" side. This allows TPD spectra to be taken without interference from the effects of electron beam damage.

The palladium catalysts were small (6×4 mm) 0.1-mm thick polycrystalline foils (Johnson Matthey, Puratronic grade 99.9975%).They were spot-welded between two stainless steel rods screwed at the end of the sample manipulator consisting of two 1/4-in. copper hollow tubes. It allowed a rotational motion so that the foil could be turned to face either the RFA, the mass spectrometer, or the leak valve doser as required.

The sample was heated resistively with currents of up to 30 A during which time the manipulator was kept cool by flowing air down the inside of the copper hollows tubes. If further cooling was required liquid nitrogen could be used instead. It is in fact important that the copper remain cool during the reaction to minimize background activity.

Sample temperature was measured by a chromel–alumel thermocouple spot-welded directly to the palladium foil. Temperature was controlled either by a simple power supply without temperature feedback or by a Eurotherm 905S temperature controller interfaced with a Hewlett Packard DC power supply. Under vacuum the temperature was precise within 0.5°C while under recirculating gasses the precision was only ± 1°C.

The cell was closed over the sample and sealed from the rest of the UHV chamber with a gold-plated copper gasket. It can be opened and closed by means of an edge-welded metal bellows powered by a hydraulic jack. When closed the hydraulic system allows a vacuum of 1×10^{-8}Torr to be maintained within the chamber while the reaction cell is pressurized above 1 atm.

Reactions were carried out in a batch mode with the reaction gasses being recirculated at 6 scc/s through a reaction loop volume of 220 scc. Gases were introduced to the reaction loop either through the gas manifold or with a syringe via a septum injection port. The procedure was to introduce from the manifold O_2, followed by Ar to pressures of 800 Torr (to prevent leaks into the reaction loop) and finally to inject a certain volume of C_2H_6 via a gas syringe. Then the reaction gasses were recirculated and mixed for several minutes with the catalyst at room temperature before the first gas sample was taken and the foil heated to reaction temperature.

The gas phase composition was measured by an Hewlett Packard 5890 Series II gas chromatograph (GC) equipped with a 15-ft Carboxen 1000 column, 60/80 mesh (Supelco), and a thermal conductivity detector (TCD). The sampling (every 21 min) is controlled by a Hewlett Packard sampler/event controller module and the signal trace is printed and integrated on a Hewlett Packard 3392A integrator. In this manner H_2, CO, CO_2, CH_4, C_2H_4, and C_2H_6 can be separated and detected. Unfortunately Ar, N_2, and O_2 separate poorly and cannot be distinguished. Furthermore, water was not detectable with this column as it just appears as a broad increase in the background.

Upon the first introduction into the vacuum chamber each new palladium foil underwent a series of sputter/burn/anneal treatments in order to remove the surface contaminants, mostly carbon and sulfur. Each side of the foil was sputtered with a Varian bombardment ion gun for 30 min with 1800 V Ar ions while being held at 500°C. This was followed by annealing the sample at the same temperature in 5×10^{-5}Torr of oxygen for 15 min and then in UHV at 600°C for 1 min. Five or more such cycles were necessary to clean a fresh foil, but generally only one such cycle was necessary to clean a used foil after reaction.

The cleanliness of the catalyst surface was ascertained by AES prior to each reaction. Furthermore, the surface area of the foil was titrated by carbon monoxide thermal desorption. Once activated the foils showed little variation in CO TPD. Nonetheless for calculation of activation energies and reaction orders the turnover frequencies were systematically normalized to the total CO TPD signal.

In fact, fresh foils displayed an increase in activity with time under reaction and varying CO TPD signatures. So in order to prepare a catalyst whose activity was invariant between reactions each foil was first preactivated by reaction at 450°C in fuel rich conditions. This reaction was carried to completion and after two or more such treatments the reaction rate became invariant to how many reactions had been performed over the catalyst. The difference in activity between a fresh and an activated catalyst was quite large, about a factor of 20.

This activation of palladium catalysts has been widely investigated in the case of methane oxidation. Along the years it has been attributed to structural changes of the catalyst (21–23), to the progressive oxidation of palladium particles (11, 14, 24, 25), to the roughening of the surface (26–28), or to carbon dissolution into bulk palladium (22, 26–29).

As the temperature of the foil is increased during reaction, the turnover frequency increases until the heat generated from the reaction is significant enough to make an impact on the temperature of the foil. For 0.004-in. thick foils, ~2 mm × 6 mm this occurs at ~425–500°C. Once this temperature is reached, the temperature of the sample increases very rapidly by several hundred degrees if the current across the foil is constant. If this input current is controlled by the Eurotherm temperature controller, then the temperature of the sample undergoes wild oscillations of several hundred degrees. Although it is possible to slightly adjust the light-off condition by adjusting the flow of the gas recirculation, the light-off phenomenon effectively excludes kinetic measurements between ~425 and 700°C.

The state of the catalyst was also periodically checked by performing a standard reaction under stoichiometric conditions at 325°C to see that the activity was unchanged.

3. RESULTS

3.1. Standard Reaction

The first reaction was run at 325°C under stoichiometric conditions of 1 : 3.5 C_2H_6 : O_2 molar ratio. In this special case the fuel/oxygen ratio remains constant as the reaction proceeds. Typically, the reaction mixture consisted of 110 Torr of oxygen and 31.5 Torr of ethane, balanced with argon to 800 Torr.

The initial turnover frequency (ToF) for CO_2 production is 11 s^{-1} (molecules of CO_2 produced per surface palladium atom per second), assuming 10^{15} surface sites per cm^2 (Fig. 1). As the reaction proceeds a decrease in the activity

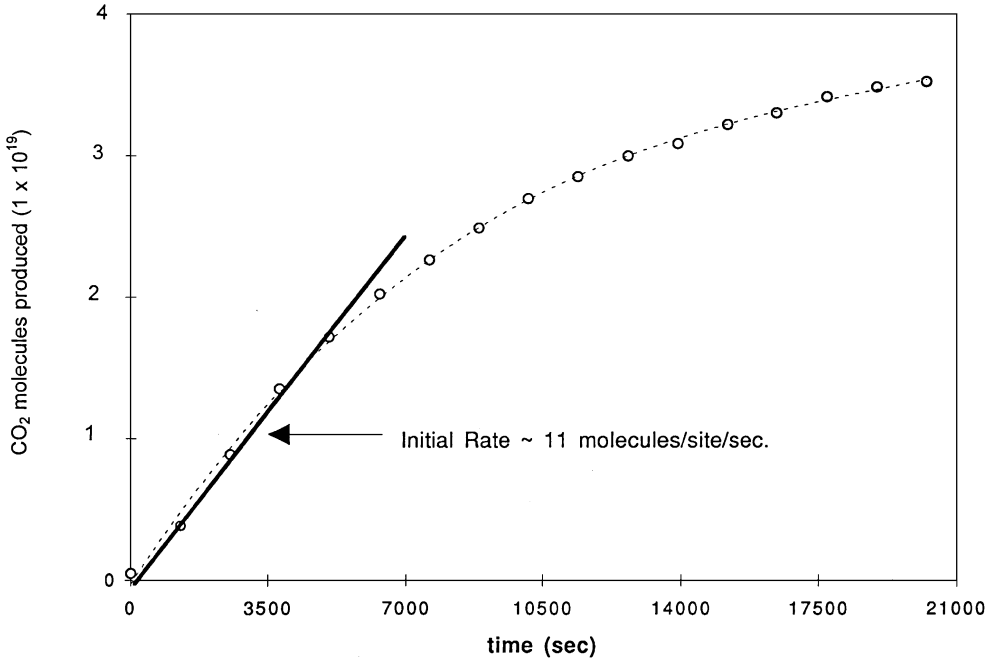

FIG. 1. CO_2 accumulation curve for ethane oxidation on palladium foil at 325°C under stoichiometric reaction conditions (110 Torr O_2, 31.5 Torr C_2H_6, balance with Ar to 800 Torr). The initial turnover rate for CO_2 formation is 11 molecules of CO_2 produced per surface palladium atom per second. It then progressively decreases as a function of time on stream, indicating either the deactivation of the catalyst or the inhibiting effect of reaction products.

can be seen, characterized by the bending over of the accumulation curve for CO_2 production as a function of time. This observation could be related either to the deactivation of the catalyst with time on stream or to a kinetic effect of both reactants and products. The former hypothesis was easily rejected when, by simply pumping out the reaction cell and starting a "new" reaction, the initial activity was restored. In fact deactivation was directly related to the poisoning effect of products accumulating with time on stream as the reaction is run in a batch reactor.

3.2. Activation of Palladium by Changes of the Surface Composition

In order to make inferences as to the state of the surface during the reaction a series of UHV and postreaction experiments were performed. Before reaction the Auger spectrum of the foil only showed palladium characterized by four peaks at 193, 243, 279, and 330 eV (Fig. 2a). However, because of the proximity of the carbon 272 eV and the palladium 279 eV peaks, it is difficult to measure the amount of carbon by Auger alone. Thus, as a further check for cleanliness, oxygen was adsorbed on the surface at room temperature. The sample was then heated while carbon monoxide and carbon dioxide desorption were monitored by mass spectrometry. At the point where no carbon monoxide or dioxide was produced, the surface was assumed to be carbon-free. This procedure was developed to correlate this "carbon-free" state with a given Auger spectral signature.

The surface area of the palladium foil was also measured before reaction by CO TPD titration in order to normalize the activity. After activation no great change was observed in the CO thermal desorption spectrum.

The oxidation state of the palladium surface is important in the combustion reaction, so it was necessary to also investigate the oxygen overlayer that remains after reaction. All postreaction Auger spectra reveal the presence of oxygen bound at the surface by peaks at 490 and 510 eV (Fig. 2b), even after reactions run under fuel-rich conditions. The ratio of the palladium 330 eV peak to the oxygen 510 eV peak ranges between 3 and 5. Corrected by the relative sensitivities of palladium and oxygen, this would correspond approximately to 1/2 to 1/3 of an oxide monolayer assuming all of the signal is from the first surface layer. Because it is most likely that the subsurface regions containing relatively more palladium and some of the Auger signal is from this region, this number should be considered a minimum coverage.

Unfortunately the electron beam also induces oxygen desorption (Fig. 2b). Thus the exact oxygen coverage cannot be determined. Moreover, it is unknown from the Auger spectrum alone whether the oxygen peak is due to PdO or Pd(OH). Furthermore, thermal desorption experiments carried out on post reaction samples and on foils with an oxide or an oxide/hydroxide overlayer prepared in situ did not show significantly different features. The surface oxide produced during the reaction appears to be quite

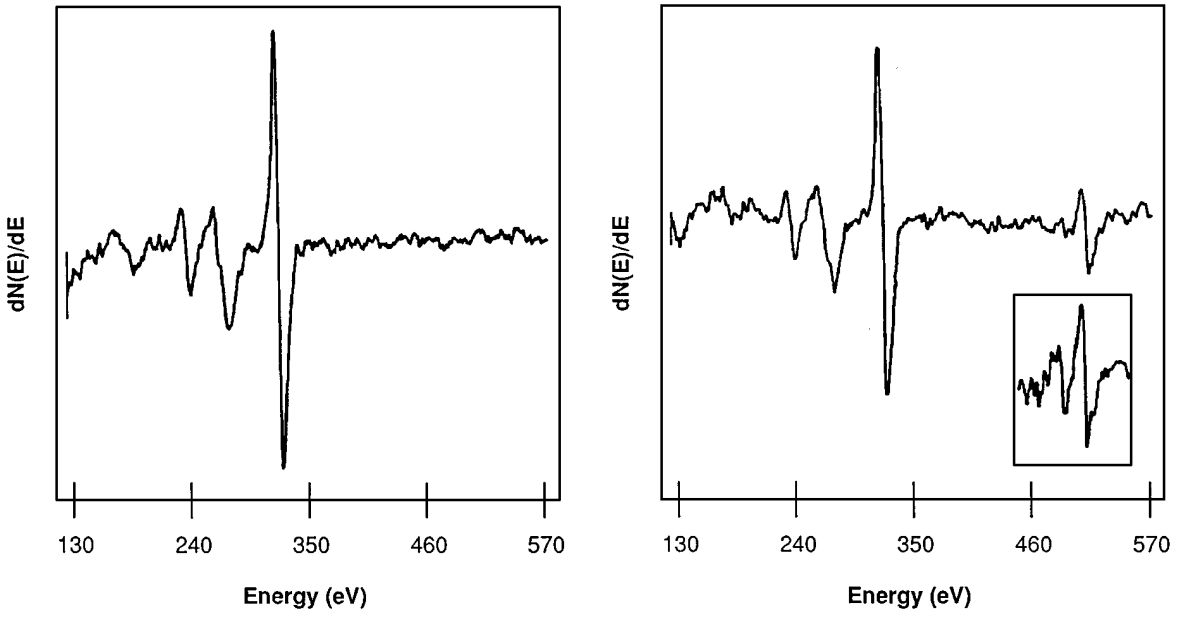

FIG. 2. (a) Auger spectrum of a clean palladium foil taken after sputtering with Ar ions at 500°C, burning in oxygen ($P = 1 \times 10^{-7}$Torr) and annealing to 600°C in vacuum. The spectrum shows the palladium signature of a clean palladium foil characterized by four peaks at 193, 243, 279, and 330 eV. (b) Auger spectra of the palladium foil after reaction at 325°C under stoichiometric conditions. The lower spectrum on the right, in the oxygen region, was taken first, before scanning the whole region from 130 to 570 eV (main spectrum in the upper part of the figure). This figure shows the existence of an oxide layer on the palladium surface after reaction. It also demonstrates the effect of the electron beam that desorbs some of the surface oxygen. Surface oxygen is characterized by two peaks at 490 and 510 eV which decrease in intensity as a function of exposure to the electron beam.

stable. There was no change in the Auger spectrum of post reaction foils until they were heated in UHV well past reaction temperatures (>600°C). Nevertheless these imply that during the reaction the surface is in large part covered by an oxide and/or hydroxide layer and that activation involves the formation of a partially oxide covered palladium metal.

3.3. Kinetic Parameters

The reaction orders in C_2H_6, O_2, CO_2, and H_2O for ethane oxidation or CO_2 production were determined at 325°C using initial rates under conditions of pseudo-zero-order kinetics. Partial pressures of C_2H_6, O_2, CO_2, and H_2O were varied one at a time from 15 to 65 Torr, 14 to 800 Torr, 3 to 24 Torr, and 3 to 13 Torr, respectively, to cover a wide range of reaction conditions from fuel rich to fuel lean.

As is common in the case of combustion reactions, determining the kinetic effect of water was more problematic. So, in order to avoid problems associated with the possibility of changing the catalyst surface, it was decided to introduce the water at high temperature (~250°C) and in the presence of ethane and oxygen. These experiments were also performed in the regime where the water vapor pressure is insufficient to initiate condensation on the walls of the reaction loop. Figures 3 and 4 show the plots of ln(ToF) versus ln(C_2H_6, CO_2, H_2O, and O_2 initial partial pressures). In the case of oxygen the direct plot of the ToF versus oxygen partial pressure, which clearly allows us to make the distinction between two different regimes, depending on the oxygen concentration (on either side of the stoichiometry), is also given in Fig. 5.

Under the conditions of this study which are under both fuel-rich, stoichiometric, and fuel-lean conditions, the combustion of C_2H_6 is first order in C_2H_6, zero order in CO_2, and minus first order in H_2O.

In the case of the oxygen dependence of the reaction rate, there is a change of the reaction order in oxygen that occurs near the stoichiometry. In fuel-rich conditions ethane combustion is minus half order in oxygen, while under fuel-lean reaction conditions the ToF is independent of the oxygen pressure. A similar trend was sometimes observed in the case of CH_4 oxidation (17, 20, 30).

The apparent activation energy for CO_2 formation was also investigated at three different oxygen concentrations. These measurements were made using the initial rates under conditions of pseudo-zero-order kinetics. It was determined to be 116 ± 3 kJ/mol under stoichiometric conditions (110 Torr O_2, 31.5 Torr C_2H_6, balance with Ar to 800 Torr) between 300 and 415°C (Fig. 6), 104 ± 5 kJ/mol under oxygen rich conditions (600 Torr O_2, 31.5 Torr C_2H_6, balance with Ar to 800 Torr) between 300 and 400°C and 189 ± 6 kJ/mol under fuel-rich conditions (60 Torr O_2, 31.5 Torr C_2H_6, balance with Ar to 800 Torr) between 300 and 350°C.

3.4. Selectivity

Even if the major combustion product is CO_2 (98.6 mol% at 10% conversion), C_2H_4 (0.9 mol% at 10% conversion),

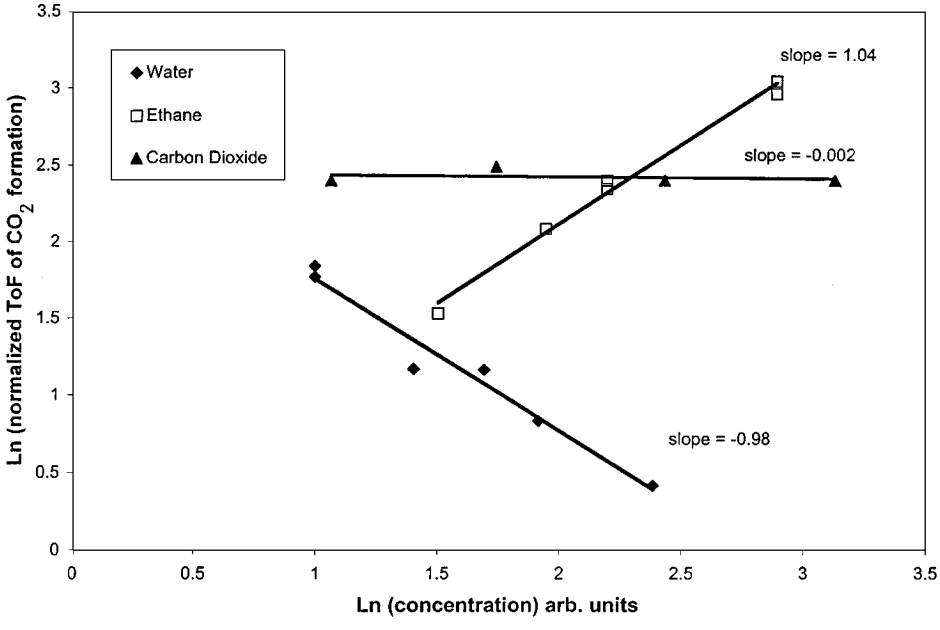

FIG. 3. Log/log plot of the turnover rate vs C_2H_6 partial pressure for the order in ethane for CO_2 production. All reactions were performed at 325°C while the partial pressure of ethane was varied from 15 to 65 Torr. The linear increase of the turnover rate with C_2H_6 partial pressure indicates a first-order reaction in ethane.

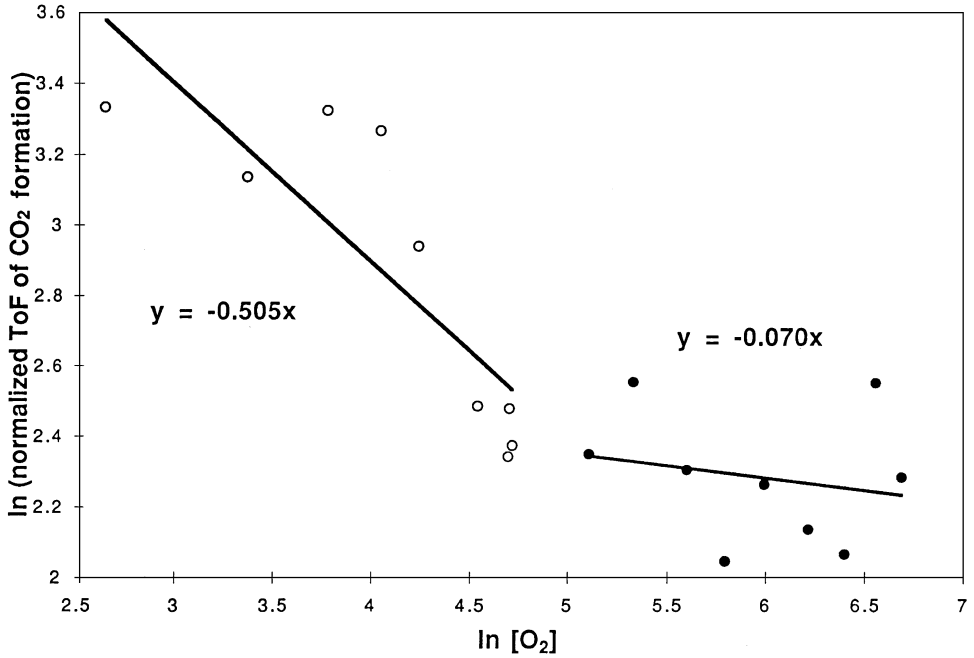

FIG. 4. Log/log plot of the turnover rate vs O_2 partial pressure for the order in oxygen for CO_2 production. All reactions were performed at 325°C and the oxygen partial pressure ranges from 14 to 800 Torr. The reaction order in oxygen is not unique over the whole range of oxygen concentration and changes at the stoichiometry from −0.5 under fuel-rich conditions to 0 in fuel-lean conditions.

and small amounts of CH_4 (0.5 mol% at 10% conversion) were also detected during reaction at 350°C under stoichiometric conditions. Furthermore, under fuel-rich conditions and above 400°C small amounts of H_2 and CO were also detected, suggestive of ethane reforming.

Figure 7 shows the accumulation curves of CO_2, CH_4, and C_2H_4 for a reaction at 350°C under stoichiometric conditions (110 Torr O_2, 31.5 Torr C_2H_6, balance with Ar to 800 Torr). The CH_4 concentration was always proportional to the CO_2 concentration. The CO_2/CH_4 ratio was nearly

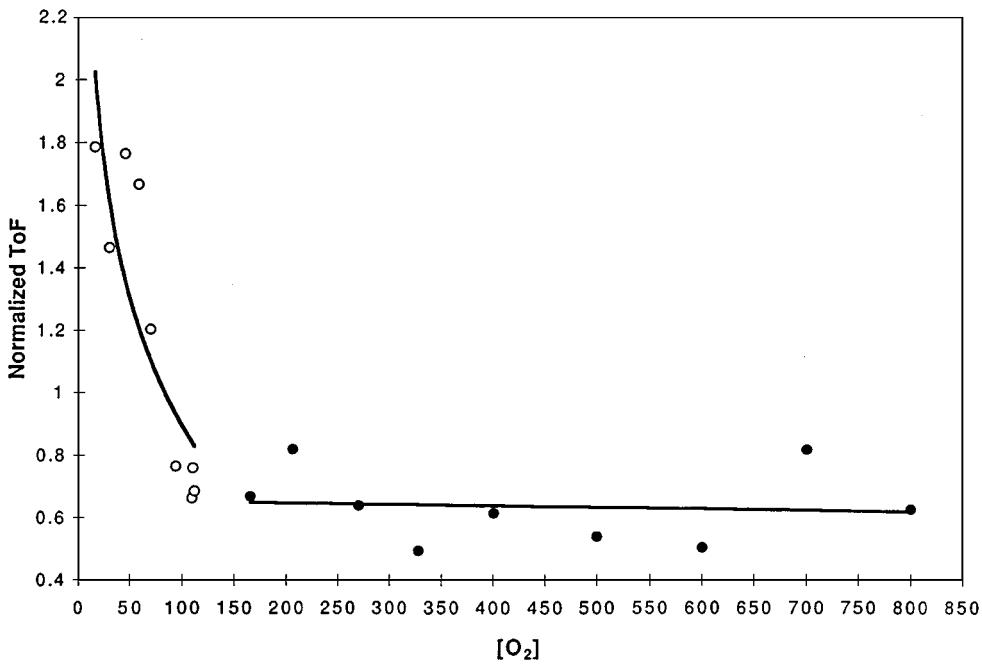

FIG. 5. Plot of CO_2 production dependence on oxygen partial pressure. Reactions performed at 325°C under 31.5 Torr C_2H_6 and 14 to 800 Torr of O_2, balanced with Ar to 800 Torr. This figure indicates the existence of two well-defined domains, depending on the oxygen partial pressure. In fuel-rich conditions the turnover frequency strongly depends on the oxygen concentration while under oxygen-rich conditions no influence is observed.

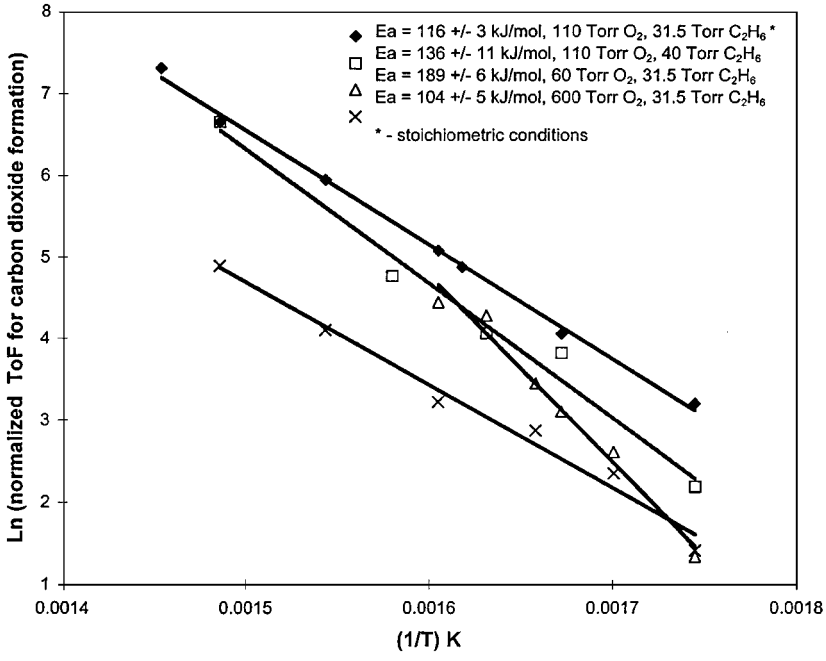

FIG. 6. Arrhenius plot for CO_2 formation under standard stoichiometric conditions between 300 and 415°C; $\Delta E^* = 116 \pm 3$ kJ/mol.

constant at 85 at all temperatures and under both fuel-rich and fuel-lean conditions. In contrast the partial pressure of C_2H_4 remained constant during the reaction. Under typical stoichiometric conditions the amount of steady state C_2H_4 is about 0.25 mol% of the initial amount of ethane. The steady state concentration of ethylene produced during ethane oxidation correlates linearly with the concentration of ethane (Fig. 8). This implies that the rate of formation of ethylene is first order in ethane initial partial pressure. So, the steady state amount of C_2H_4 linearly

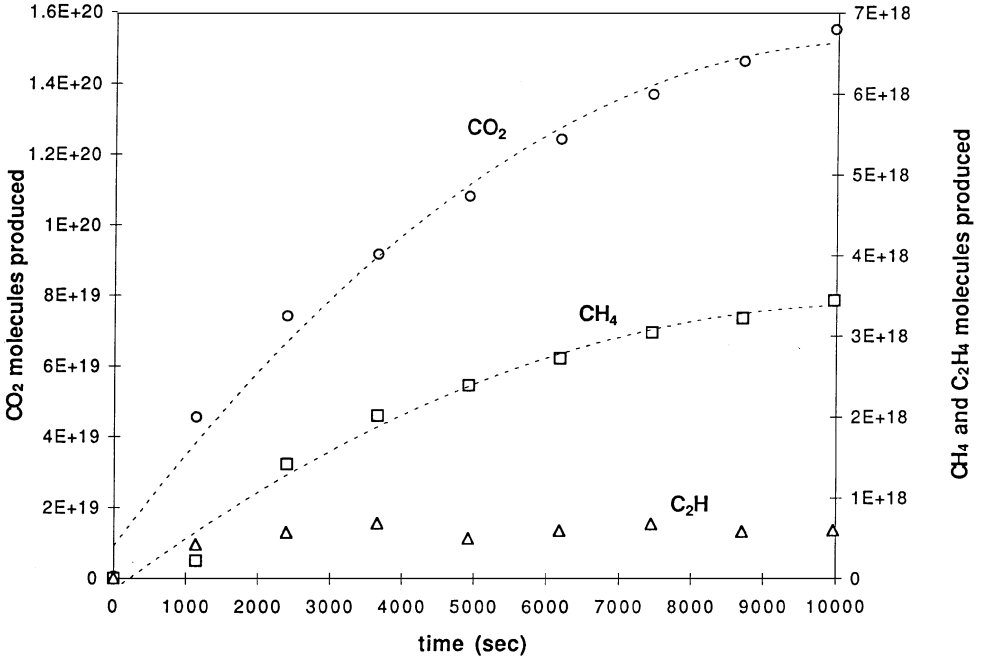

FIG. 7. CO_2, C_2H_4, and CH_4 accumulation curves for ethane oxidation on palladium foil at 350°C under stoichiometric conditions (110 Torr O_2, 31.5 Torr C_2H_6, balance with Ar to 800 Torr). At 10% conversion the gas phase composition is 98.6 mol% CO_2, 0.9 mol% C_2H_4, and 0.5 mol% CH_4. The CO_2/CH_4 ratio is constant at about 85 and the steady state amount of C_2H_4 represent 0.25 mol% of the initial amount of ethane.

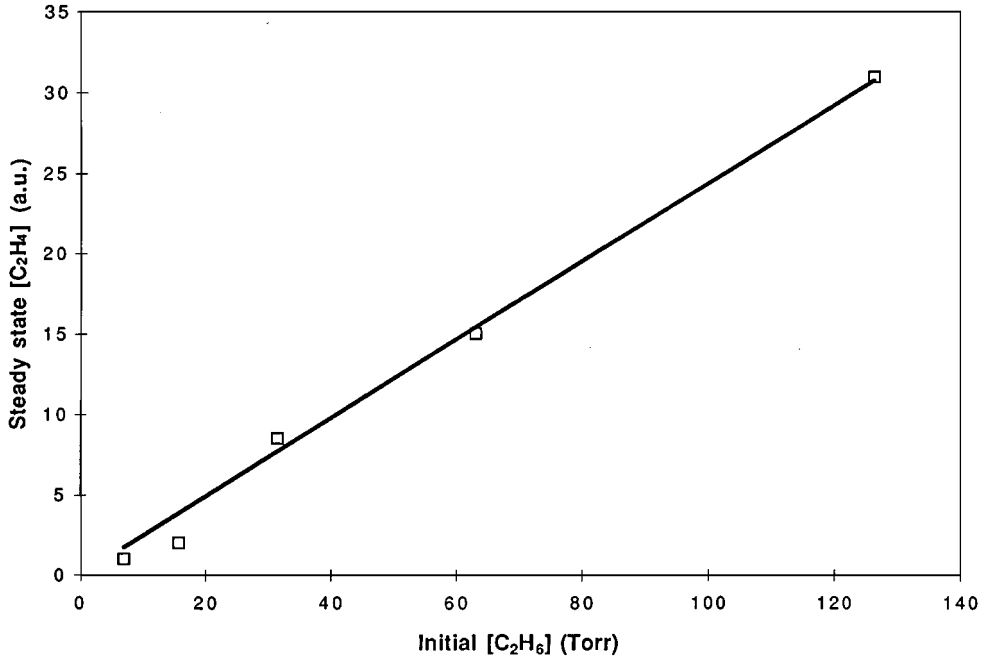

FIG. 8. Dependence of the steady state C_2H_4 concentration on the initial C_2H_6 partial pressure. Reactions performed at 325°C under 110 Torr O_2. Ethylene steady state concentration depends linearly on ethane initial partial pressure. The formation of ethylene is first order in ethane.

increases when going from fuel-lean to fuel-rich reaction conditions.

In fact ethylene has been recently reported as the major product in ethane oxidation over metal oxides (31–33). High selectivity for ethylene was also measured during ethane combustion at very high flow rate or low contact time (34–37).

3.5. Ethylene Combustion

Ethylene combustion to carbon dioxide and water was also studied in order to determine the possible total amount of ethylene produced during the reaction. Experiments were performed in a batch reactor at 325°C with 110 Torr O_2 and 3 Torr of ethylene. Those conditions were chosen to minimize the inhibiting kinetic effects of oxygen and water. In this way the reaction rate was always pseudo-zero order in oxygen and water.

The reaction was carried to completion and the decay of ethylene signal appears to follow first-order kinetics in ethylene. The ToF was determined to be $1.2 \times 10^{-3} s^{-1}$ in these conditions. Given that the dependence of the rate of combustion of ethylene is first order in ethylene up to a very low level of ethylene, the ToF of ethylene formation is calculated to be $0.6\ s^{-1}$ under standard reaction conditions. Thus, 11% of the ethane would be converted to ethylene as an intermediate before its eventual complete oxidation to CO_2, while the rest of the ethane converted is directly oxidized to CO_2 and H_2O.

4. DISCUSSION

Ethane oxidation is strongly exothermic ($\Delta G^0 = -1442$ kJ/mol) and the relative stability of the alkane is high, as compared to partially oxidized species. It is then reasonable to assume, as is well accepted for CH_4 oxidation (11–16), that the rate determining step is the scission of the first C-H bond. This is in line with the observation that CO_2 production is first order in ethane concentration in a broad range around the stoichiometric mixture. This assumption is also supported by the correlation seen between the C-H bond strength and the rate of combustion (12, 17, 18, 30, 38).

Characterization of the surface of the sample before and after reaction clearly shows that the active surface is partially oxygen covered.

The independence of the rate on the gas phase concentration of CO_2 indicates that, once the product desorbs, it does not readsorb and no longer affects the mechanism. This is in disagreement with the inhibiting effect of CO_2 reported in the case of methane oxidation (11, 12, 19). Indeed in our case the apparent cleanliness of the palladium surface after the reaction indicates that during the reaction the catalyst is not covered with a strongly bound carbonaceous surface species, but instead the major species are PdO and/or $Pd(OH)_x$. This suggestion is supported by the negative order dependence of the rate of CO_2 production on the gas phase concentrations of H_2O and, under fuel rich conditions, of O_2.

Taken together our experimental observations are consistent with a mechanism in which the ethane adsorbs with the scission of a C-H bond in the rate-determining step, followed by the rapid oxidation of the surface intermediates. The fast oxidation of non-alkane intermediates over noble metals (39–44) or hydrocarbons radicals (39, 45, 46) has been observed in numerous surface science studies.

Two different regimes on either part of the stoichiometry have been distinguished from the reaction rate dependence on the oxygen partial pressure. This can be related to a change in the surface composition, the palladium surface becoming more and more oxidized as the oxygen partial pressure increases. In fact there is always a significant oxygen peak in the Auger spectrum after reaction even for those performed under the most fuel-rich conditions. Thus, it is reasonable to assume that there are two possible sites and mechanisms for the initial C-H bond cleavage depending on the oxygen coverage on the surface (12). The first would occur on a partially reduced heterogeneous site Pd-PdO [1] and the second on a PdO-PdO site [1′].

$$C_2H_6 + Pd + PdO \rightarrow CO_2, H_2O, C_2H_4, CH_4 \qquad [1]$$

$$C_2H_6 + 2\,PdO \rightarrow CO_2, H_2O, C_2H_4, CH_4. \qquad [1']$$

The former site, containing reduced palladium, would be more active than the latter and control the kinetics under fuel-rich conditions. As one moves from fuel-rich to oxygen-rich reaction mode, the surface becomes more and more oxidized and the less active oxide ensemble site dominates the kinetics. In this regime the reaction is then independent of O_2 partial pressure which is in agreement with the experimental observations.

With these assumptions for the slow step, depending on the oxygen coverage, the rate of ethane oxidation is given by

$$r_1 = -\left(\frac{d[C_2H_6]}{dt}\right)_1 = k_1 \times [C_2H_6] \times \theta_{Pd} \times \theta_{PdO} \qquad [1]$$

$$r_{1'} = -\left(\frac{d[C_2H_6]}{dt}\right)_{1'} = k_{1'} \times [C_2H_6] \times (\theta_{PdO})^2, \qquad [1']$$

where θ_* and θ_O are the coverages of Pd and PdO sites.

Assuming a rapid equilibrium of the surface with gas phase water and oxygen,

$$Pd + PdO + H_2O \rightarrow 2\,Pd(OH) \qquad [A]$$

$$2\,Pd + O_2 \rightarrow 2\,PdO. \qquad [B]$$

Then the relations that govern the coverages of surface species are

$$K_A = \left(\frac{\theta^2_{Pd(OH)}}{[H_2O] \times \theta_{Pd} \times \theta_{PdO}}\right),$$

$$K_B = \left(\frac{\theta^2_{PdO}}{[O_2] \times \theta^2_{Pd}}\right),$$

and $\theta_* + \theta_O + \theta_{OH} = 1$.

So in fuel rich conditions, if both Pd and PdO are required for the dissociation of the first C-H bond, the rate is proportional to $\theta_{Pd}\theta_{PdO}$ and is given by

$$r_1 = \frac{k_1 \times [C_2H_6]}{\left(2 + A^2 + B + 2AB^{1/2} + \frac{2A}{B^{1/2}} + \frac{1}{B}\right)},$$

where $A = (K_A \times [H_2O])^{1/2}$ and $B = (K_B \times [O_2])^{1/2}$.

Thus, under fuel-rich conditions the reaction rate should be first order in ethane, minus first order in water, and minus half order in oxygen. This is in agreement with the experimental results.

For reactions under excess oxygen the surface is almost completely covered with PdO and the rate is then proportional to $(\theta_{PdO})^2$ and given by

$$r_{1'} = \frac{k_{1'} \times [C_2H_6]}{\left(1 + \frac{A^2}{B} + \frac{2A}{B^{1/2}} + \frac{2A}{B^{3/2}} + \frac{2}{B} + \frac{1}{B^2}\right)},$$

where $A = (K_1 \times [H_2O])^{1/2}$ and $B = (K_2 \times [O_2])^{1/2}$.

In this case interpretations are more difficult as the relative values of A and B are unknown. Nevertheless, as the partial pressure of oxygen [B] increases, the surface becomes completely oxidized and the reaction order in oxygen goes to zero as all the other terms become small compared to 1. This result is consistent with what is observed experimentally.

In both cases the results are consistent with a mechanism where the rate-determining step is the activation of the first C-H bond with formation of C_2H_5 as an intermediate.

It should be noted that because both A and B contain equilibrium constants, they are functions of the temperature. Thus the temperature of the reaction would be expected to play a significant role in determining the surface species concentration, that is the concentration of the two sorts of C-H cleavage sites. The apparent activation energies for the two regimes should reflect the equilibrium number of the appropriate active site. This in fact was observed, with a higher apparent activation energy under fuel-rich conditions.

A first look to the fact that the higher activation energy is obtained for the most active system could be surprising. Nevertheless, this could be explained by realizing that the apparent activation energy also carries information about

the surface composition. In this case high activities were measured and a lot of hydroxyls are expected on the surface. As Pd(OH) is inactive for C-H bonds activation (12), the partially reduced site Pd-PdO needs to be regenerated. This occurs by recombinations of two hydroxyls, desorption of water, and regeneration of the active Pd-PdO ensemble. But it is known that water dissociative adsorption is easier on an oxidized surface (47, 48). Thus, this could explain how, on a partially reduced surface (fuel-rich conditions), the heat of desorption of water (regeneration of the active site) appears in the overall apparent activation energy.

Finally, ethylene is easier to activate than ethane and is burned at 325°C on the same catalyst at a rate 100 times that of ethane under standard conditions. As a result ethylene appears only as a steady state intermediate. Its formation and presence imply that a dehydrogenation step of the ethane molecule, probably to form C_2H_5, is involved in the overall oxidation process. Methane, on the other hand, is far more stable than ethane and can accumulate as a reaction product.

CONCLUSIONS

Ethane oxidation over palladium exhibits two different kinetic regimes, one fuel rich and the other fuel lean. It is proposed that microscopic difference between these two regimes is the nature of the active site at which the first C-H bond is broken to form C_2H_5 and a hydroxyl group on the surface. Under reducing conditions the palladium at the surface can be in any form, Pd, PdO, and Pd(OH). Dual atom sites of Pd metal and PdO are believed to be the most active sites and more readily available under fuel-rich conditions. As the partial pressure of either water or oxygen increase, the number of such Pd–PdO sites available decrease until the overall combustion activity of the foil is governed by the less active but more numerous fully oxidized PdO sites. At 325°C this crossover occurs near stoichiometric conditions. This can be seen by the change in the order of reaction in oxygen from −0.5 to 0 and in the activation energy from 189 kJ/mol to 116 kJ/mol and 104 kJ/mol that accompanies the change from oxygen-lean to stoichiometric and oxygen-rich conditions. Although it is not completely certain what causes the higher activation energy under oxygen-lean conditions, this observation is consistent with the hypothesis of a partially reduced active site that must be regenerated by the desorption of water. This would require that the recombination of OH species to desorb water contributes to the apparent activation energy of the overall reaction.

The primary product of ethane combustion under our conditions was carbon dioxide. However, the small amounts of ethylene observed imply a dehydrogenation step in the combustion process. Ethylene is observed only in small, steady state amounts because its rate of combustion is much greater than that of ethane as shown by our experiments. Nevertheless, ethylene was determined as an intermediate in the process of ethane complete oxidation, accounting for about 11% of the carbon dioxide produced. The nearly constant ratio of methane to carbon dioxide under all reaction conditions suggests that the reaction mechanisms for the formation of these two products share the same rate-determining step. Also, the fact that the production of methane is first order in ethane strongly suggests an intramolecular reaction. The low temperature of the reaction would also seem to preclude the role of gas phase radicals in this mechanism.

ACKNOWLEDGMENTS

This work was supported by the French Ministry of Foreign Affairs and by the Director, Office of Energy Research, Office of Basic Energy Sciences, Material Sciences Division, U.S. Department of Energy under Contract DE-AC03-76SF00098.

REFERENCES

1. Davy, H., *Philos. Trans. R. Soc. London* **1**, 45 (1817).
2. Davy, H., *in* "The Collected Works of Sir Humphrey Davy" (J. Davy, Ed.), Vol. 6, pp. 81–88. Smith, Elder, Corn Hill, London, 1840.
3. Pfefferle, W. C., Brit. Patent 814752 (1974); U.S. Patent 3928961 (1975).
4. Pfefferle, W. C., Heck, R. M., Carrubba, R. V., and Roberts, G. W., ASME Paper 75-WA/Fu. 1 (1975).
5. Saint-Just, J., and der Kinderen, J., *Catal. Today* **29**, 387 (1996).
6. Trimm, D. L., *Appl. Catal.* **7**, 249 (1983).
7. Ismagilov, Z. R., and Kerzhentsev, M. A., *Catal. Rev.-Sci. Eng.* **32**, 51 (1990).
8. Prasad, R., *Catal. Rev.-Sci. Eng.* **26**(1), 1 (1984).
9. Mamedov, E. A., and Cortes Corberan, V., *Appl. Catal. A* **127**, 1 (1995).
10. Schmidt, L. D., and Huff, M., *Catal. Today* **21**, 443 (1994).
11. Ribeiro, F. H., Chow, M., and Dalla Betta, R. A., *J. Catal.* **146**, 537 (1994).
12. Burch, R., and Hayes, M. J., *J. Mol. Catal. A* **100**, 13 (1995).
13. Farrauto, R. J., Hobson, M. C., Kennelly, T., and Waterman, E. M., *Appl. Catal. A: General* **81**, 227 (1992).
14. Salomonsson, P., Johansson, S., and Kasemo, B., *Catal. Lett.* **33**, 1 (1995).
15. Burch, R., and Loader, P. K., *Appl. Catal. A: General* **122**, 169 (1995).
16. Deutschmann, O., Behrendt, F., and Warnatz, J., *Catal. Today* **21**, 461 (1994).
17. Yao, Y.-F. Y., *Ind. Eng. Chem. Proc. Res. Dev.* **19**, 293 (1980).
18. Hiam, L., Wise, H., and Chaikin, S., *J. Catal.* **10**, 272 (1968).
19. Pfefferle, L. D., Dyer, M., and Crosley, D. R., *in* "Proc. Central States Sect. Combust. Instit., *1987*, p. 394.
20. Firth, J. G., and Holland, H. B., *Faraday Soc. Trans.* **65**, 1121 (1969).
21. Garbowski, E., Feumi-Jantou, C., Mouaddib, N., and Primet, M., *Appl. Catal. A: General* **109**, 277 (1994).
22. Baldwin, T. R., and Burch, R., *Appl. Catal.* **66**, 359 (1990).
23. Burch, R., and Urbano, F. J., *Appl. Catal. A: General* **124**, 121 (1995).
24. Hicks, R. F., Qi, H., Young, M. L., and Lee, R. G., *J. Catal.* **122**, 295 (1990).
25. Briot, P., and Primet, M., *Appl. Catal.* **68**, 301 (1991).
26. Haack, L. P., and Otto, K., *Catal. Lett.* **34**, 31 (1995).
27. König, D., Weber, W. H., Poindexter, B. D., McBride, J. R., Graham, G. W., and Otto, K., *Catal. Lett.* **29**, 329 (1994).
28. Otto, K., Hubbard, C. P., Weber, W. H., and Graham, G. W., *Appl. Catal. B: Environmental* **1**, 317 (1992).

29. Baldwin, T. R., and Burch, R., *Catal. Lett.* **6**, 131 (1990).
30. Drozdov, V. A., Tysrulnikov, P. G., Popovskii, V. V., Bulgakov, N. N., Moroz, E. M., and Galeev, T. G., *React. Kinet. Catal. Lett.* **27**, 425 (1985).
31. Desponds, O., Keiski, R. L., and Somorjai, G. A., *Catal. Lett.* **19**, 17 (1993).
32. Burch, R., and Swarnarkar, R., *Appl. Catal.* **70**, 129 (1991).
33. Amorebieta, V. T., and Colussi, A. J., *J. Am. Chem. Soc.* **118**, 10236 (1996).
34. Schmidt, L. D., and Huff, M., *Catal. Today* **21**, 443 (1994).
35. Schmidt, L. D., Huff, M., and Bharadwaj, S. S., *Chem. Eng. Sci.* **49**, 3981 (1994).
36. Goetsch, D. A., and Schmidt, L. D., *Science* **271**, 1560 (1996).
37. Dietz III, A. G., and Schmidt, L. D., *Catal. Lett.* **33**, 15 (1995).
38. Schwartz, A., Holbrook, L. L., and Wise, H., *J. Catal.* **21**, 199 (1971).
39. Solymosi, F., Kovács, I., and Révész, K., *Catal. Lett.* **27**, 53 (1994).
40. Dannetun, H., Lundström, I., and Petersson, L.-G., *Surf. Sci.* **193**, 109 (1988).
41. Calhorda, M. J., Lopes, P. E. M., and Friend, C. M., *J. Mol. Catal. A* **97**, 157 (1995).
42. Lambert, R. M., Ormerod, R. M., and Tysoe, W. T., *Langmuir* **10**, 730 (1994).
43. Watanabe, K., Uetsuka, H., Ohnuma, H., and Kunimori, K., *Appl. Surf. Sci.* **99**, 411 (1996).
44. Ormerod, R. M., and Lambert, R. M., *Catal. Lett.* **6**, 121 (1990).
45. Bugyi, L., Oszkó, A., and Solymosi, F., *J. Catal.* **159**, 305 (1996).
46. Solymosi, F., *Catal. Today* **28**, 193 (1996).
47. Thiel, P. A., and Madey, T. E., *Surf. Sci. Rep.* **7**, 211 (1987).
48. Yuzawa, T., Higashi, T., Kubota, J., Kondo, J. N., Domen, K., and Hirose, C., *Surf. Sci.* **325**, 223 (1995).